Otto-von-Guericke-Universität
Magdeburg

Simulation of motion artifacts in magnetic resonance imaging

Author:
Chandrakanth Jayachandran Preetha
Examiner:
Prof. Dr. rer. nat. habil. Oliver Speck
Supervisor:
Hendrik Mattern, M. Sc.

Enrollment Number:
217961

April 23, 2019

Contents

1 Introduction **2**
1.1 Motivation 2
1.2 Objective 2

2 Background **3**
2.1 MR Image Acquisition Process 3
2.2 Effect of Motion on k-Space 4

3 Motion Simulation Framework **5**
3.1 Motion Corruption Block 6
3.1.1 3D Affine Transformation 7
3.1.2 Simulation of Gradient Field Nonlinearity 7
3.1.3 Simulation of Parallel Imaging 9
3.1.4 FFT of Manipulated Images and Substitiution of K-space Lines 11
3.2 Image Reconstruction 11
3.3 Quality Assessment 12

4 Methods **12**
4.1 Evaluation of quality of interpolation 13
4.2 Motion Amplitude Experiment 13
4.3 Higher Order Effects 14

5 Results **15**

6 Conclusion **17**

1 Introduction

1.1 Motivation

Motion artifacts are an inherent problem to MRI technology. This is primarily due to the prolonged data acquisition time necessary for most MR imaging sequences. Motion artifacts could degrade image quality and thereby affect clinical diagnosis. The sources of motion in subjects can be classified as (i) periodic involuntary motion, e.g. cardiac and respiratory motion, (ii) sudden involuntary motion caused by sneezing, coughing, yawning and semi-regular motion such as swallowing and blinking, (iii) conscious motion of body parts, e.g. due to discomfort [1]. Variation in the intensity or position of the subject due to subject motion leads to inconsistencies in the MR signal between different signal acquisition steps.

Retrospective motion correction methods modify the raw MR data or image data after acquisition. They require detection of object motion either by tracking the object or from the raw data itself. A framework that could generate motion corrupted images based on flexible motion trajectory could be useful for developing data-driven methods for motion detection and retrospective motion correction.

1.2 Objective

The objective of this project is to develop a framework for simulation of subject motion in MR images. The framework aims to enable simulation of macroscopic 3D motion of the subject with a flexible motion trajectory for cartesian MRI. Rigid body assumption is made for the subject and only inter-scan motion is simulated. In order to reproduce effects of subject motion in parallel imaging methods, multi-coil set up is also incorporated. Existing frameworks for simulation of motion artifacts in MR images generally do not include higher order artifacts due to gradient field non-linearity and coil sensitivity profile . Excluding these higher order effects from the motion simulation framework could lead to over simplification and motion artifact correction methods developed using such data could fail to produce satisfactory results on real motion corrupted MRI data. A flexible and modular structure is envisioned for the framework so that image artifacts produced by these different sources can be separately studied. The framework would also allow the quantification of changes in the image and k-space domain using suitable metrics.

2 Background

2.1 MR Image Acquisition Process

In MR imaging the acquired signals are spatially encoded by the application of electro-magnetic fields and the raw data are stored in two dimensional k-space arrays. The contribution of different frequency waves to the image is indicated by the magnitude of the points in the k-space and the phase of these points indicate how the waves are positioned in the image. The coordinates of each measurement point is given by the gradient moment [2].

$$k(t') = \int_0^{t'} \gamma G(t) dt \tag{1}$$

where γ is the gyromagnetic ratio, G(t) is the strength of the gradient as a function of time, and t′ is the time at which a data sample is collected. The gradient fields cause continuous change of the coordinates and the signal is sampled at discrete times. The spatial frequency spectra of objects with smooth intensity variations are characterized by components close to origin of the k-space (see Fig.1). The final image is obtained by applying an inverse Fourier transformation on the acquired k-space data.

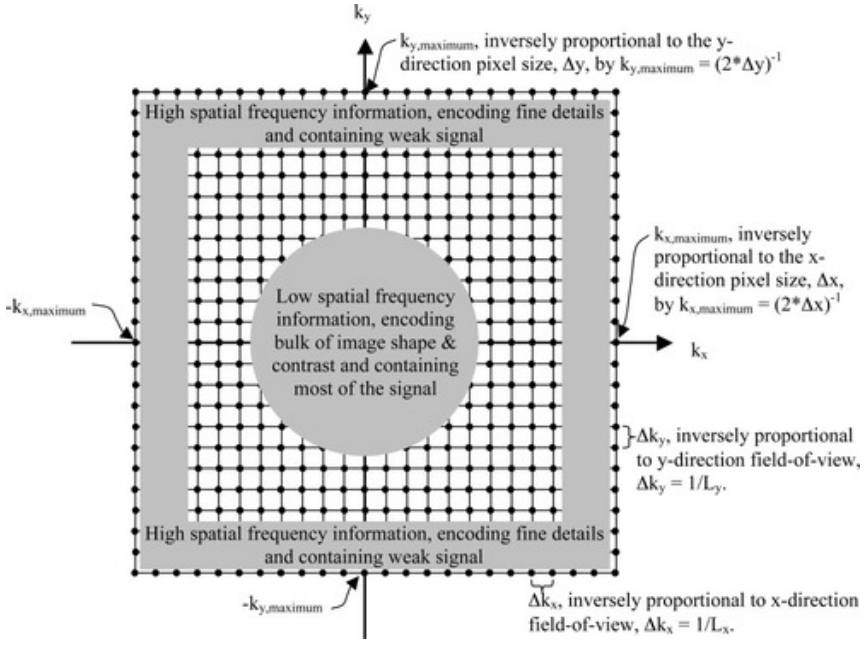

Figure 1: Features of k-space (from [2])

2.2 Effect of Motion on k-Space

The artifacts induced by object motion in MR images are a combination of the following fundamental effects: blurring of object edges, ghosting (partial or complete replica of the image), signal loss due to spin dephasing and the appearance of undesired strong signals [3]. In Cartesian sampling schemes, the signal acquisition is much faster in frequency encoding direction compared to acquisition in the phase encoding direction. As a result the motion-induced artifacts appear mainly along the phase encoding direction of the spatial domain image reconstruction, independent of the the direction of motion.

The relation between rigid body motion in the spatial domain and its influence on the k-space data is well-defined. Rigid motion is the combination of translational and rotational motions. The properties of k-space allows the separation of the effects of translation and rotation of a rigid body on the k-space data. According to Fourier Shift Theorem, translation in the spatial domain results in a linear phase ramp in the k-space data in the direction of the motion. Equation (2) describes the phase corruption for a given k-space sample where k_x and k_y are the spatial frequency values, and Δx and Δy are the relative displacement of the object [4].

$$\Delta\Phi(k_x, k_y) = 2\pi(k_x\Delta x + k_y\Delta y) \tag{2}$$

According to the Fourier Rotation Theorem, rotation of the object in spatial domain results in identical rotation of the k-space data with the rotation axis through the origin. This results in local Nyquist violations in the k-space (see Figure 2), producing ghosting and streaking artifacts in the reconstructed image.

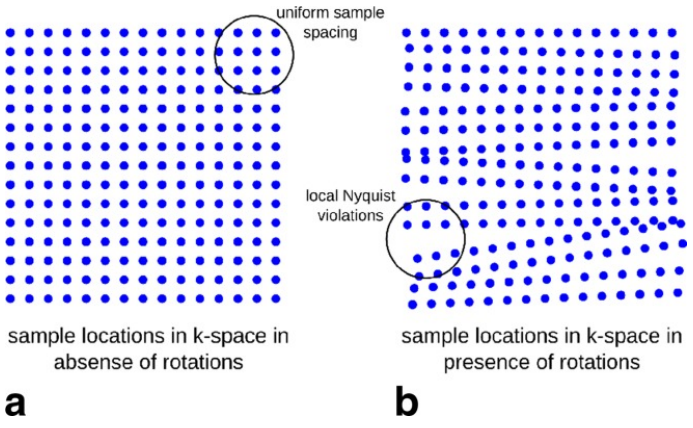

Figure 2: (a) The signals are arranged in a uniform grid in the absence of rotation. (b) Object rotation causes nyquist violations (from [3])

3 Motion Simulation Framework

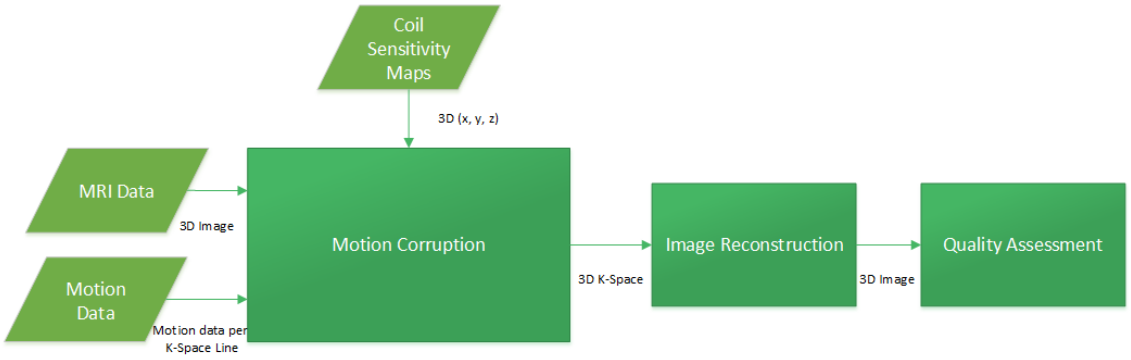

Figure 3: Overview of the motion simulation framework

The proposed framework illustrated in Figure 3 simulates subject motion in MR images using rigid body motion data. The subject motion is simulated as rigid motion with six degrees of freedom, consisting of a 3D translation vector and three rotation angles. The 3D rigid body motion is simulated and the object motion is tracked by determining the relative displacement and change in orientation. The motion data is stored in a tabular format with the following information : i) 3D translation vector that indicates the relative displacement, ii) axis and angle of rotation of the imaging volume which indicates the change in orientation. The number of entries in the motion table depends on the number of slices in the image volume and the extent of the image in the phase encode direction. The entries in the table are arranged assuming that the data is acquired sequentially along the phase encode direction(s).

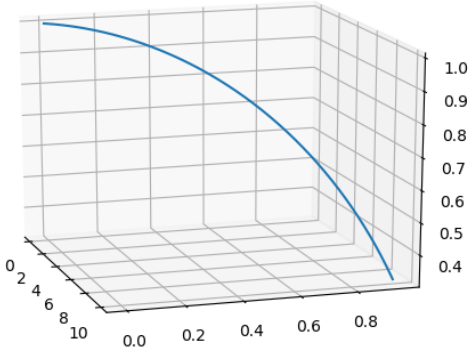

Figure 4: 3D sinusoidal motion generated using the rigid body motion simulator

The motion corruption block receives the 3D image volume, tabular motion data and coil sensitivity map as input. Image reconstruction is performed on the motion-corrupted k-space data generated by the motion corruption block. These images with motion artifacts are then compared with the original image for quality assessment using suitable metrics.

3.1 Motion Corruption Block

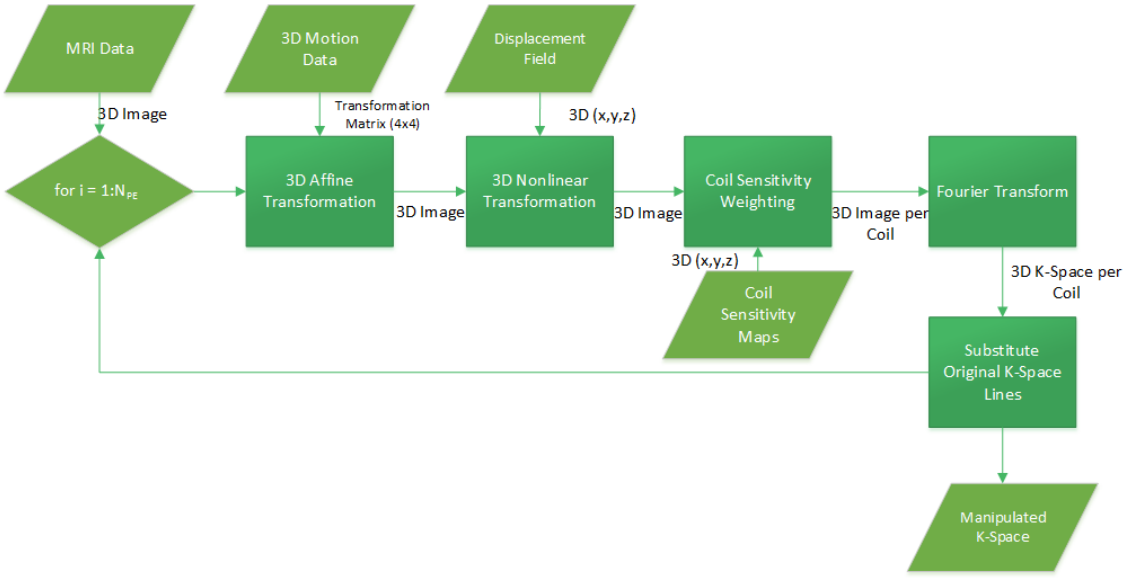

Figure 5: k-Space Manipulation

The motion corruption block (see Figure 5) induces motion artifacts with the help of rigid transformation of the original image volume. It is assumed that the image volume is aligned with the physical coordinate and therefore they have the same orientation and center. Instead of directly manipulating the k-space data, the image volume is transformed repeatedly according to the motion trajectory obtained from the motion table to simulate rigid body motion. A distortion field is subsequently applied on the transformed image in order to simulate the effects of gradient field non-linearity. The resultant image is weighted by coil sensitivity profiles which are then Fourier transformed to obtain raw data for different coils. After each iteration, the k-space of the coil sensitivity weighted original image is merged with those of the transformed image by exchanging specific samples from the original k-space with the corresponding samples of the transformed image. Once all the original k-space lines are replaced for all coils, the resultant raw data is equivalent to an image acquisition

in which subject motion causes misplacement of raw data values in each of the phase encoding steps.

3.1.1 3D Affine Transformation

Affine transformation is a linear mapping which preserves points, straight lines and planes. They preserve collinearity and and ratio of distances. Affine transformations can represent translations, rotations, scaling and shear [5]. These spatial transformations can be represented by matrix multiplication of a point represented as a vector. The use of matrix representation also allows factoring of a complex transformation into a set of simpler transformations. They enable encapsulation of complex transforms and store them in a compact form. Forming products of transformation matrices is referred to as a composition of matrices. The affine transformations of a point $P = (P_x, P_y, P_z)$ can be expressed as

$$P_t = \begin{pmatrix} r_{xx} & r_{yx} & r_{zx} & \Delta x \\ r_{xy} & r_{yy} & r_{zy} & \Delta y \\ r_{xz} & r_{yx} & r_{zz} & \Delta z \\ 0 & 0 & 0 & 1 \end{pmatrix} \begin{pmatrix} P_x \\ P_y \\ P_x \\ 1 \end{pmatrix} \tag{3}$$

The above 4×4 matrix can represent all affine transformations. The upper-left 3×3 sub-matrix represents the rotation applied by the transform and the last column of the matrix represents translations along the three axes. Rigid body motion has six degrees of freedom, translation in three perpendicular axis combined with change in orientation through rotation about three perpendicular axes. Shearing and scaling effects are neglected due to the rigid body assumption. The change in orientation of the object is represented in the motion table using the angle and axis of rotation, using which a composite 3×3 rotation matrix is generated. The rotation matrix is combined with the translation vector to create a 4×4 homogeneous transformation matrix.

3.1.2 Simulation of Gradient Field Nonlinearity

Accurate spatial encoding of MR signals requires linear variation in the gradient field. Magnetic field inhomogeneity and non-linearity of the gradient field causes signal misplacement and geometric distortions. Linearity of the gradient field generally decreases as distance to the isocenter increases.Thus, distortion caused by the gradient field nonlinearity are spatially varying and increase with the distance to the isocenter. Subject motion during imaging with non linear gradient field also results

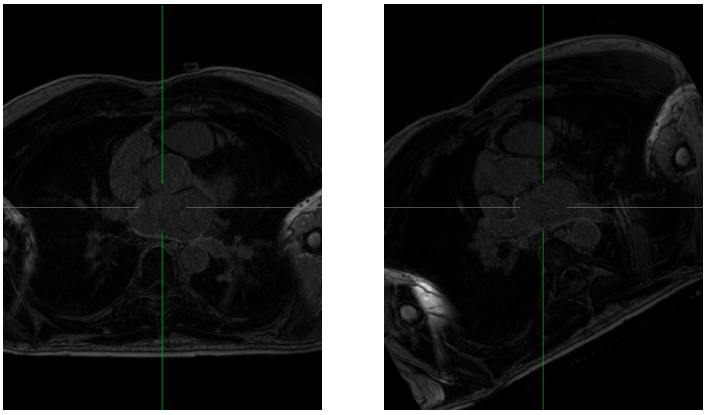

(a) Original image (b) Transformed image

Figure 6: Application of affine transform (global shift and rotation) on an MR image

in blurring in addition to spatial distortion since the imaging data of the object acquired at different locations within the non-linear will have different geometry [6].

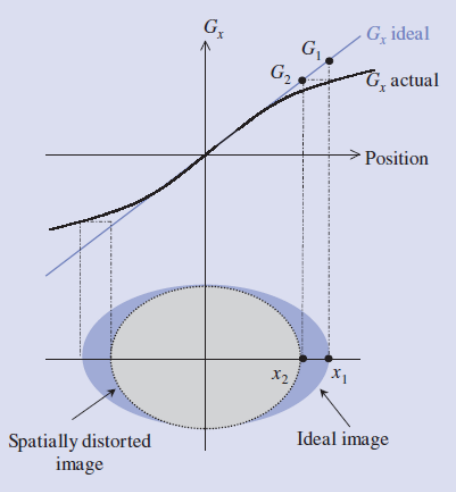

Figure 7: Geometric distortion due to gradient field nonlinearity(from [7])

The simulation of these artifacts in the image requires the application of nonlinear transformations. These types of image transformations are called image warping. These transformations are generally used for correcting image distortions or for creative purposes. In general these transformations can be represented as:

$$x' = T_x(x, y) \qquad y' = T_y(x, y) \tag{4}$$

where T_x and T_y are nonlinear functions of the input coordinates (x,y).These transformations cannot be represented as simple matrix multiplication in homogeneous coordinates. Many nonlinear distortion effects can be modelled accurately by representing T_x and T_y as second-order polynomials [8]. A distortion field which represents a nonlinear distortion effect is applied on the image to simulate the geometrical distortion caused by gradient field nonlineartiy. The displacement field is generated based on the model for radial distortion effect [9].

$$P_u = P_d + (P_d - P_c)(k_1 r^2 + k_2 r^4 + K_3 r^6 + ...) \tag{5}$$

where P_u is a pixel coordinate in the undistorted image, P_d is a pixel coordinate in the distorted image, P_c is the center of the distortion, $r = ||P_d - P_c||$ and k_i are the coefficients of the distortion.

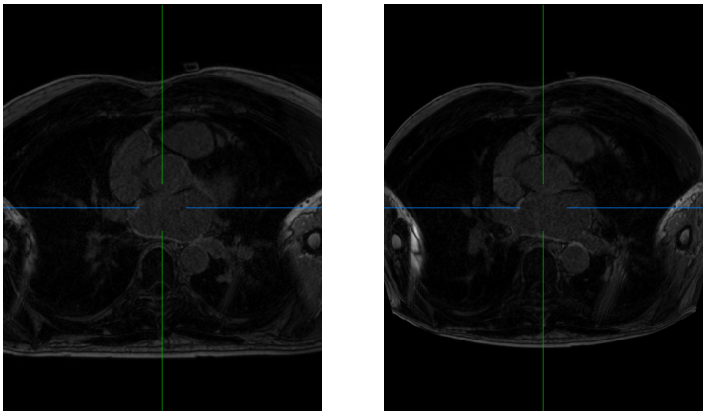

(a) Original image (b) Distorted image

Figure 8: Application of displacement field on an MR image

3.1.3 Simulation of Parallel Imaging

MRI acquisitions are time consuming since the acquisition of K-space data is done line by line and the pulse sequence has to be repeated for each of the lines so that the full data set can be built up. In parallel imaging mode, the information about coil positions and sensitivities can be used to reduce the number of phase encoding steps and thereby speed up imaging. The spatial encoding originally achieved by the use of spatial encoding gradients is now partially substituted by evaluating data from different coil elements with spatially varying coil sensitivity profiles. The reduction in phase encoding steps and imaging time is achieved by reducing the sampling density.

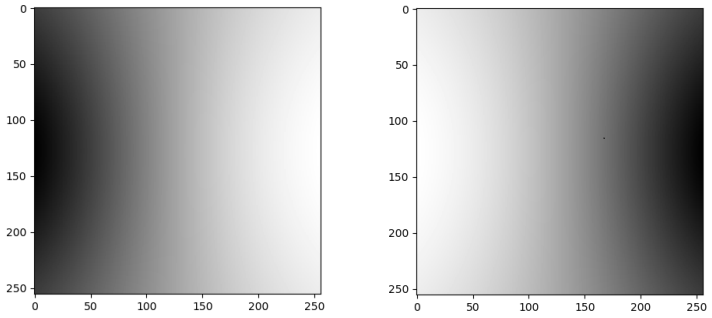

Figure 9: Birdcage coil sensitivity maps

The simulation of parallel imaging process and inclusion of the effects of multi-coil set up requires the generation of receiver coil sensitivity maps. The framework allows the generation of birdcage sensitivity profile for the receiver coils. The size of the coil sensitivity map can be adjusted based on the dimension of the input 3D image and the number of coils in the set up can be varied. The framework also allows the relative radius of the birdcage coil to be adjusted. Figure 9 shows examples of generated coil sensitivity maps.

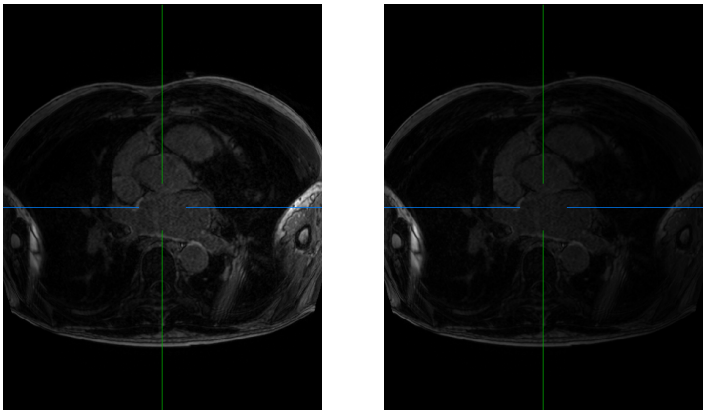

(a) Coil 1 image (b) Coil 2 image

Figure 10: Coil sensitivity weighted images

The 3D image which undergoes affine transformation followed by warping to simulate rigid body motion and gradient nonlinearity effect respectively, are weighted by the coil sensitivity maps to produce different images corresponding to each of the coils. The examples of coil sensitivity weighted images are shown in Figure 10. Subject motion during data acquisition causes change in coil sensitivities with respect to

the moving object. Interactions between subject motion and receive coils leads to variation in signal phase and amplitude, resulting in shading artifacts.

3.1.4 FFT of Manipulated Images and Substitiution of K-space Lines

After each transformation of the 3D image, the k-space of the corresponding coil sensitivity weighted images are determined using FFT. The k-space lines of the coil sensitivity weighted copies of the original image are replaced by those of the manipulated image iteratively after each transformation. The raw data corresponding to an image acquisition with subject motion is obtained once the complete sequence of transformations are performed and all the k-space lines are replaced.

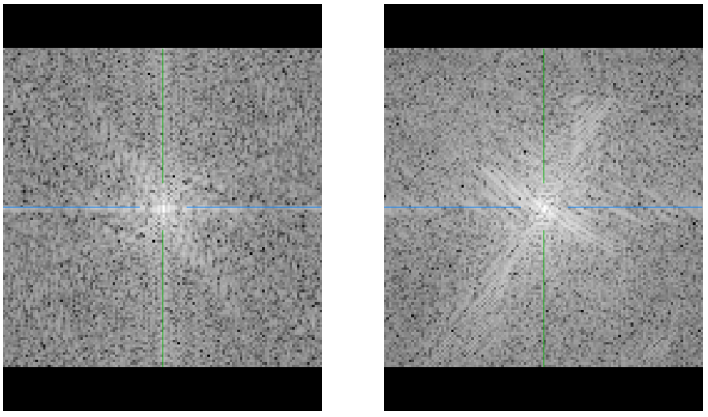

(a) K-space of original image

(b) K-space generated after motion corruption

Figure 11: Motion corrupted k-space

3.2 Image Reconstruction

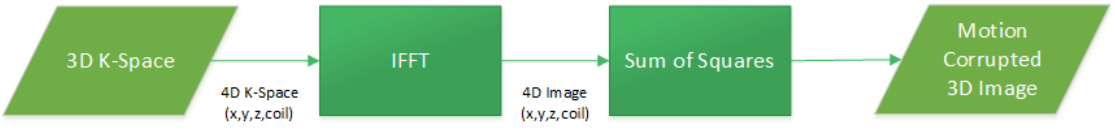

Figure 12: Image reconstruction from motion corrupted k-space

Figure 12 describes the image reconstruction pipeline. Inverse fourier transform is performed on the manipulated k-space of all the coils to obtain the images corresponding to each coil. The images from multiple coils are then combined using an

image domain reconstruction method, square root of sum of squares reconstruction. Figure 13 shows an example of an image reconstructed using square root of sum of squares method from the motion corrupted raw data where k-space manipulation was performed based on a 3D sinusoidal motion pattern.

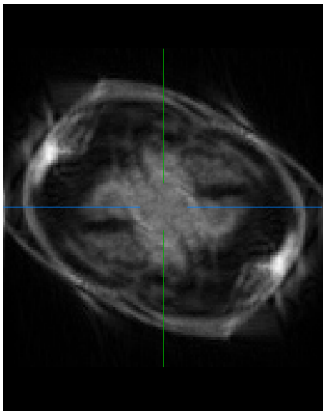

Figure 13: Image reconstructed from motion corrupted k-space

3.3 Quality Assessment

In the final stage of the framework, the motion corrupted image is compared with the corresponding uncorrupted image. It allows the evaluation of the contribution or influence of different factors towards motion artifacts. Structural similarity (SSIM) index [10], which is based on the computation of luminance, contrast and structural terms is used as the comparison metric. The SSIM value ranges from 0 to 1 (perfect copy). In addition to SSIM, root mean square error (RMSE) is also used for comparison. It is a quadratic scoring rule which measures the average magnitude of the error. Similar comparison is also possible with the raw data of individual coils.

4 Methods

Experiments were conducted to evaluate the effect of i) image interpolation ii) motion amplitude on motion artifacts, iii) gradient nonlinearity and multi-coil data acquisition on motion artifacts. Motion corrupted images were generated using motion patterns of varying amplitude and with the inclusion of higher order effects in the motion simulation pipeline. These motion corrupted images were then compared with corresponding original image devoid of motion artifacts. The image

volume used for the experiments is a T1-weighted image acquired with a magnetization prepared rapid gradient echo (MPRAGE) sequence. The original 3D image volume was resized to $128 \times 128 \times 24$ to reduce computational effort. While applying a phase ramp on k-space data allows for sub-pixel object translation, achieving the same in image domain usually requires upsampling of the image prior to applying image transformations. The framework overcomes this limitation by defining the image as a set of points on a grid occupying a physical region in space. This method enables sub-pixel translation and also allows both object translation and rotation to be performed simultaneously in the image domain.

4.1 Evaluation of quality of interpolation

The choice of the interpolation method is crucial for the motion corruption framework. If the interpolation method compromises the image quality, the accuracy of the motion simulation framework will be adversely affected. Linear interpolation method was chosen for both rigid body transformations and nonlinear transformations as it provided the best trade off between accuracy and computational efficiency [11]. The quality of the interpolation method was tested by rotating the image 360 times by 1 degree and comparing the final image with the original image using SSIM as the metric.

4.2 Motion Amplitude Experiment

In order to study the effects of translation and rotation of the object separately, motion patterns consisting of pure translation and rotation of varying amplitude were generated. Rigid body transformations were then applied to the imaging volume based on these motion patterns. The image volume was shifted along the axial plane in the phase encode direction and rotation was performed about the axis perpendicular to the axial plane. Higher order effects were excluded from the pipeline for this experiment. An interleaved pattern was used for the application of motion artifacts, rigid body transformations were applied in such a way that only specific lines (every 15^{th} k-space line in case of translation and every 25^{th} line in case of rotation) along the phase encoding was motion corrupted. Figure 14 shows examples of motion pattern used to study the influence of motion amplitude on the corrupted image.

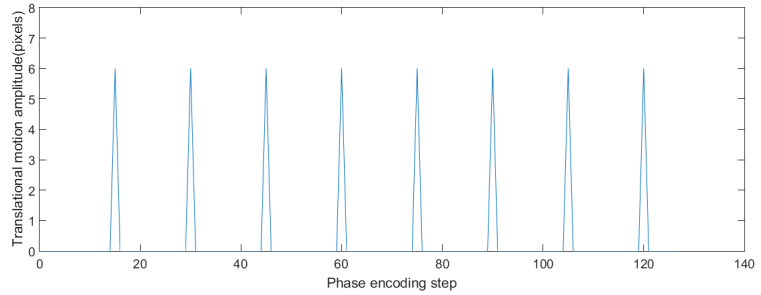

(a) Motion amplitude plot for translational motion pattern

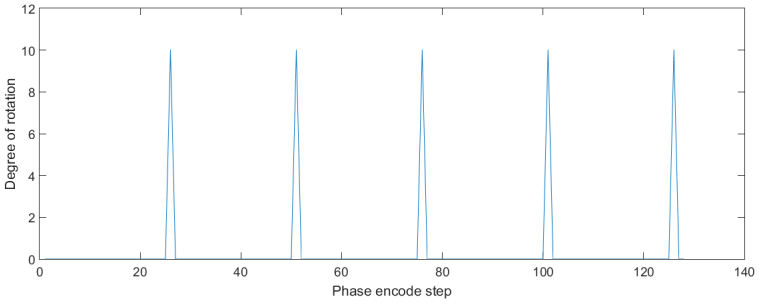

(b) Motion amplitude plot for rotational motion pattern

Figure 14: Motion amplitude over phase encoding steps

4.3 Higher Order Effects

The contribution of gradient field nonlinearity and multi-coil raw data acquisition towards distortion in the image domain was studied by including these effects along with rigid body transformation in the motion corruption block. These effects were applied separately and also in combination to understand their influence on motion artifacts. The motion pattern used for motion corruption consisted of a combination of translation along the axial plane and rotation about the axis perpendicular to the axial plane. The amplitude of translation and rotation were 10 pixels and 10 degrees respectively. Motion artifacts were then generated in the image by exchanging k-space lines between the transformed image volume and the original image volume. An interleaved motion pattern was generated where only every 25^{th} k-space line was motion corrupted.

In order to study the influence of multi-coil acquisition method in image quality, a parallel image reconstruction scheme was simulated using two birdcage coil sensitivity maps with a relative radius of 1.5 with respect to the FOV. The gradient nonlinearity effect was simulated using a 3D distortion field. The distortion field was generated with its center coinciding with the center of the image volume and

coefficients of distortion (see equation 5) $k_1 = 0.0000001$, $k_2 = 0.0000000000001$ and $k_3 = 0.0000000000001$.

5 Results

The result of the interpolation experiment is shown in Figure 15. The image generated after 360 rotations of 1 degree each had an SSIM score of 0.7455 with respect to the original image.

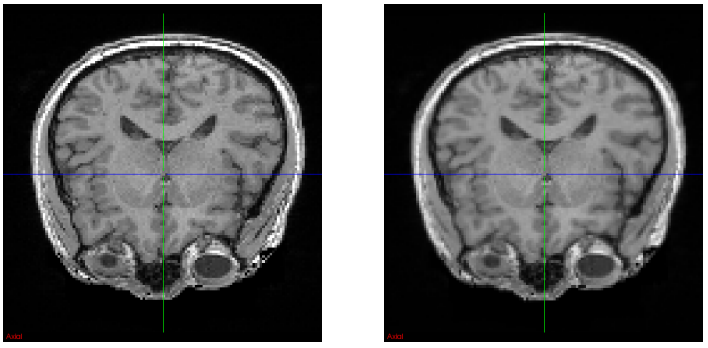

(a) Original image

(b) Image obtained after 360 rotations

Figure 15: Comparison of original image with the interpolated image

The results of evaluation of motion amplitude on motion artifacts are shown in Figure 16 and Figure 17. It was observed that with increase in amplitude of object translation, the image quality deteriorated. Similar results were also observed in the case of motion artifacts generated by pure rotational motion, the image quality metric deteriorated at higher amplitudes of rotational motion. Figure 18 shows the result of different amplitudes of translation and rotation of the object on the corrupted image.

The comparison of SSIM indices and root mean square error (RMSE) for motion corrupted images with different combination of artifacts is given in Table 1. The SSIM values of the different images varied considerably based on the applied higher order effects while the RMSE metric was relatively insensitive to the change in applied effect. The comparison of SSIM indices indicates that the use of multi-coil scheme and application of gradient nonlinearity effect resulted in deterioration of image quality. The application of multi-coil scheme and gradient nonlinearity effect resulted in decrease in SSIM value by 4% and 63% respectively. The image quality metrics were at the lowest when the two effects were applied simultaneously in the

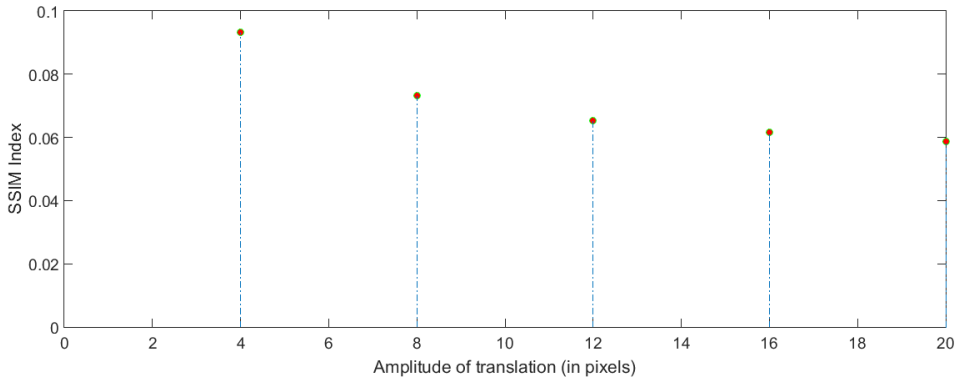

Figure 16: Comparison of SSIM index for object translation

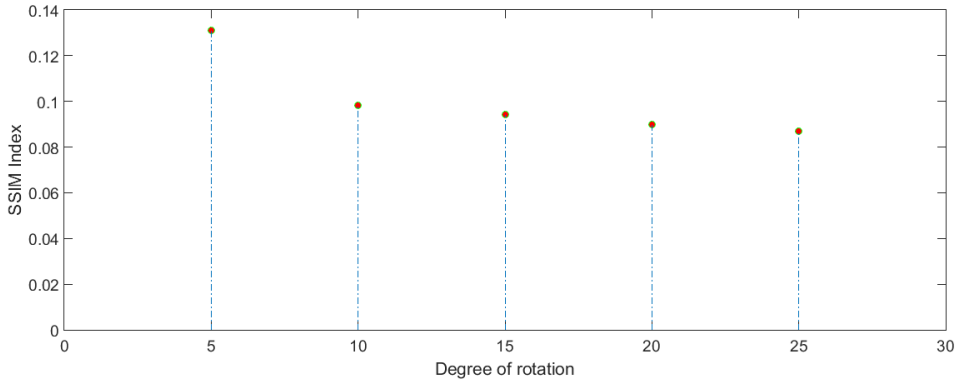

Figure 17: Comparison of SSIM index for object rotation

motion simulation framework. The result of application of higher order effects in different combination is showed in Figure 19.

Effects Applied	**SSIM Index**	**RMSE**
No higher order effects	0.1154	9.6070
Multi-coil setup	0.1108	9.6617
Gradient nonlinearity	0.0425	10.2204
Gradient nonlinearity and Multi-coil setup	0.0337	10.2302

Table 1: Comparison of structural similarity index and root mean squared error of motion corrupted images

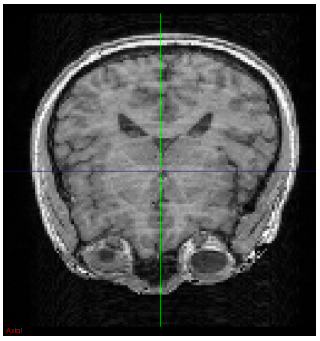

(a) Motion corrupted with minimum object translation

(b) Motion corrupted with maximum object translation

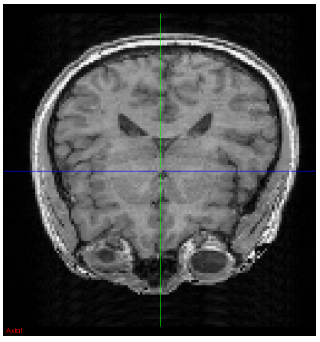

(c) Motion corrupted with minimum object rotation

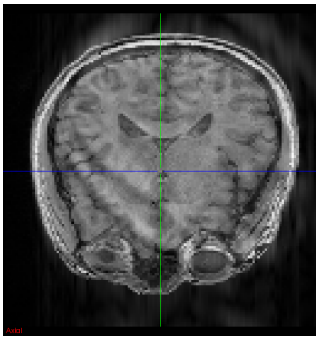

(d) Motion corrupted with maximum object translation

Figure 18: Comparison of motion corrupted images with different motion amplitudes

6 Conclusion

The proposed framework allows the simulation of rigid body motion artifacts in MR imaging. It enables the use of a flexible motion trajectory which could facilitate the study of motion corruption of MR images with complex motion patterns. In addition to raw data corruption due to subject motion, the framework also allows for including the effects of gradient field nonlinearity and multi-coil image acquisition. The modular structure of the framework allows the user to include these effects in any combination.

The interpolation method gave satisfactory results when tested with repeated image transformations. The framework prevents accumulation of interpolation error since all object poses in a motion trajectory are generated by transforming the original image, thereby minimising the effect of interpolation errors.

The motion amplitude experiments show that higher amplitude of object motion causes higher levels of motion degradation in the reconstructed image. Substantial change in SSIM score was observed between motion corrupted images generated with lowest and highest amplitude of object motion. At highest amplitude of translational motion, the SSIM score decreased by 36 percent compared to the SSIM score at lowest level of object motion. Similar decrease in SSIM score was also observed in case of the rotational motion experiment.

Even though the experiments identified gradient nonlinearity to have a stronger effect, there are certain factors that needs be taken into consideration. The experiments on higher order artifacts were conducted using only two coils, typically more coils with stronger variations are used in parallel imaging. Thus, the effect is expected to scale with the number of coils and more localized coil profiles. Furthermore, no scan acceleration was used in the experiments. Potentially, if parallel imaging is used for image acceleration, coil profiles are used to unwrap the images and the effect of motion on these reconstructions from under-sampled k-space could be enhanced. Also, distortion caused by the gradient field nonlinearity are spatially varying and increase with the distance to the isocenter, so object position is an important factor. Both gradient nonlinearity and relative motion of coil sensitivity profiles are expected to be more important for high amplitude motion and for unintentional small-scale motion their effect should be negligible.

The framework allows for varying the parameters of the multi-coil acquisition scheme, including the number and size of receive coils. The parameters used to generate the distortion field could also be varied to simulate different degrees of gradient nonlinearity. Future work would aim to utilize these capabilities of the framework to quantify these effects and their effect on motion artifacts.

The limitations of the framework include the two stage transformations of the image, a homogeneous transformation to simulate rigid body motion and a nonlinear transformation to include gradient nonlinearity effect. Future work also aims to adopt the framework as a synthetic data generation tool for deep learning based motion artifact detection. Correction of motion corrupted raw data is another potential extension of the framework.

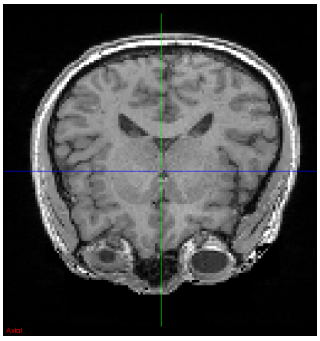

(a) Original Image

(b) No higher order effects

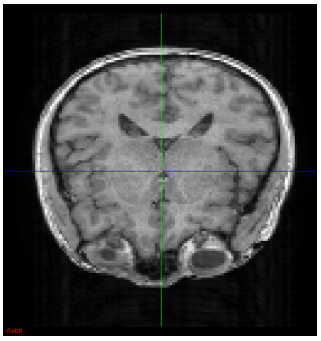

(c) Rigid transform with nonlinear gradient field

(d) Rigid transform with multi-coil setup

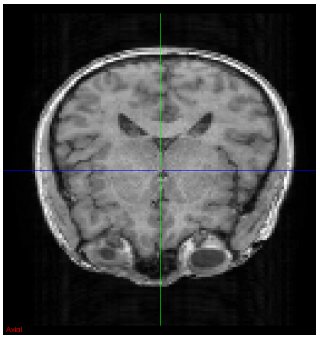

(e) Rigid transform with nonlinear gradient field and multi-coil setup

Figure 19: Visualization of effects of gradient field nonlinearity and multi-coil setup on motion corruption

References

[1] F. Godenschweger, U. Kägebein, D. Stucht, U. Yarach, A. Sciarra, R. Yakupov, F. Lüsebrink, P. Schulze, and O. Speck. Motion correction in mri of the brain. *Phys Med Biol*, 61(5), Mar 2016.

[2] Cynthia B. Paschal and H. Douglas Morris. K-space in the clinic. *Journal of Magnetic Resonance Imaging*, 19(2):145–159.

[3] Maxim Zaitsev, Julian Maclaren, and Michael Herbst. Motion artifacts in mri: A complex problem with many partial solutions. *Journal of Magnetic Resonance Imaging*, 42(4):887–901.

[4] Edward Brian Welch, Joel P. Felmlee, Richard L. Ehman, and Armando Manduca. Motion correction using the k-space phase difference of orthogonal acquisitions. *Magnetic Resonance in Medicine*, 48(1):147–156.

[5] George Wolberg. *Digital Image Warping*. IEEE Computer Society Press, Los Alamitos, CA, USA, 1st edition, 1994.

[6] Uten Yarach, Chaiya Luengviriya, Appu Danishad, Daniel Stucht, Frank Godenschweger, Peter Schulze, and Oliver Speck. Correction of gradient nonlinearity artifacts in prospective motion correction for 7t mri. *Magnetic Resonance in Medicine*, 73(4):1562–1569.

[7] D.W. McRobbie, E.A. Moore, M.J. Graves, and M.R. Prince. *MRI from Picture to Proton*. Cambridge University Press, 2017.

[8] C.J. Solomon and T.P. Breckon. *Fundamentals of Digital Image Processing: A Practical Approach with Examples in Matlab*. Wiley-Blackwell, 2010. ISBN-13: 978-0470844731.

[9] Duane C. Brown. Close-range camera calibration. *PHOTOGRAMMETRIC ENGINEERING*, 37(8):855–866, 1971.

[10] Kieran G. Larkin. Structural similarity index ssimplified: Is there really a simpler concept at the heart of image quality measurement? *CoRR*, abs/1503.06680, 2015.

[11] Image interpolation - simpleitk prototype 0.11 documentation. `https://simpleitk-prototype.readthedocs.io/en/latest/user_guide/transforms/plot_interpolation.html`.

[12] Julian Maclaren, Michael Herbst, Oliver Speck, and Maxim Zaitsev. Prospective motion correction in brain imaging: A review. *Magnetic Resonance in Medicine*, 69(3):621–636.